International Journal of Heat and Fluid Flow 30 (2009) 198–210

Contents lists available at ScienceDirect

International Journal of Heat and Fluid Flow

journal homepage: www.elsevier.com/locate/ijhff

Tip gap height effects on flow structure and heat/mass transfer over plane tip of a high-turning turbine rotor blade

Sang Woo Lee *, Hyun Suk Moon, Seong Eun Lee

School of Mechanical Engineering, Kumoh National Institute of Technology, 1 Yangho-dong, Gumi, Gyeongbuk 730-701, Republic of Korea

ARTICLE INFO

Article history:
Received 17 May 2008
Received in revised form 21 December 2008
Accepted 26 December 2008
Available online 31 January 2009

Keywords:
High-turning turbine rotor blade
Tip gap height
Tip gap vortices
Tip surface heat/mass transfer
Tip gap flow model

ABSTRACT

The effects of tip gap height-to-chord ratio, h/c, on the flow structure and heat/mass transfer over the plane tip surface of a large-scale high-turning turbine rotor blade have been investigated for h/c = 1.0%, 2.0%, 3.0% and 4.0%. For near-wall tip gap flow visualizations, a high-resolution oil film method is employed, and the naphthalene sublimation technique is used for local heat/mass transfer rate measurements. From the tip surface visualizations, a pair of vortices named "tip gap vortices" is identified in the leading edge region within the tip gap. The overall tip gap flow is characterized not only by the tip gap vortices but also by the flow separation/re-attachment process along the pressure-side tip edge. Within the separation bubble, there exist complicated near-wall flows moving toward a mid-chord flow converging area. With increasing h/c, the tip gap vortices, the flow separation/re-attachment, and the converging flows within the separation bubble tend to be intensified. In general, higher thermal load is found along the loci of the tip gap vortices and along the re-attachment line, while lower thermal load is observed behind the tip gap vortex system and near the mid-chord flow converging area. Heat/mass transfer characteristics with the variation of h/c are discussed in detail in conjunction with the tip gap flow features. Based on the flow visualizations and heat/mass transfer data, new realistic tip gap flow models have been proposed for h/c = 1.0 and 4.0%.

1. Introduction

The clearance gap between the tip surface of a turbine rotor blade and the adjacent stationary casing wall forms a narrow flow passage. Due to the presence of pressure difference between the pressure and suction-sides of the blade, there exists a leakage flow through the tip gap. This leakage flow leads to additional aerodynamic losses and thermal loading to the blade tip. The tip region is exposed to hot combustion gases on the pressure, suction, and tip surfaces and thus is difficult to cool, which could result in tip burnout. Therefore, it is very important to understand detailed flow and heat transfer characteristics over the tip surface for efficient tip cooling schemes.

Many investigations have been conducted on the tip leakage flow development and the aerodynamic loss generation through the tip gap. Sjolander and Amrud (1987) investigated the effect of leakage flow on the blade loading of a linear cascade. They showed the existence of separation lines on the cascade endwall and of separation bubbles on the tip surface caused by the leakage flow. Bindon (1989) investigated the detailed development of tip clearance loss within a linear turbine cascade passage and quantified the contributions made by mixing, internal gap shear flow and endwall/secondary flow. He also suggested a conceptual flow model in the tip gap flow region. Moore et al. (1989) investigated the effect of Reynolds number on flow and heat transfer in turbine tip gaps for an idealized two-dimensional tip geometry, and found a large separation off the sharp edge of the blade tip corner at high Reynolds numbers. Yamamoto (1989) discussed the mechanism of three-dimensional flow and of the associated losses occurring near the tip endwall region of a linear turbine cascade with various tip gaps and incidences. He reported that at small tip gap, leakage flow tends to follow the pressure gradient within the tip gap, while with increasing the tip gap, the inertial force of the inlet endwall flow appears to become an important factor in determining the leakage flow vector in the front part of the tip. Bindon and Morphis (1992) found that radiusing and contouring the blade at gap inlet eliminate the tip inlet separation bubble and reduce internal gap loss but create higher mixing loss to give almost unchanged overall loss coefficients when compared with the simple sharp-edged plain tip blade. Tallman and Lakshminarayana (2001) carried out numerical simulations of plane tip leakage flows for h/c = 1.0% and 2.5%, and discussed various flow physics related to the tip leakage flows.

After early studies on idealized turbine blade tip models (Chyu et al., 1989; Metzger and Rued, 1989; Rued and Metzger, 1989; Moore et al., 1989; Metzger et al., 1991), many investigators were interested in heat transfer on the plane tip of actual turbine

* Corresponding author. Tel.: +82 54 478 7296; fax: +82 54 478 7319.
E-mail address: swlee@kumoh.ac.kr (S.W. Lee).

0142-727X/$ - see front matter © 2009 Elsevier Inc. All rights reserved.
doi:10.1016/j.ijheatfluidflow.2008.12.009

Nomenclature

b	axial chord	s	span
c	chord	Sc	Schmidt number (Sc = ν/D)
D	diffusion coefficient of naphthalene in air	Sh	Sherwood number (Sh = $h_m c/D$)
h	tip gap height	U_∞	inlet free-stream velocity
h_m	local mass transfer coefficient	xyz	cascade coordinates
Nu	Nusselt number	α	thermal diffusivity of air
Pr	Prandtl number (Pr = ν/α)	ν	kinematic viscosity of air
Re	inlet Reynolds number (Re = $U_\infty c/\nu$)		

geometries. Ameri et al. (1999) carried out numerical simulations on the effects of tip clearance and casing recess on heat transfer and stage efficiency of a turbine rotor blade of h/b = 0%, 1%, 1.5% and 3%. The result showed an increase in the thermal load on the all heat transfer surfaces considered due to enlargement of the clearance gap. Bunker et al. (2000) conducted measurements over the plane tip of a power generation gas turbine with a 110° turning angle. They reported heat transfer coefficient distributions on the plane tip surfaces with both sharp and rounded edges. Ameri and Bunker (2000) performed numerical simulations on the heat transfer and flow for the same geometry that Bunker et al. (2000) employed. They reported detailed tip surface heat transfer coefficient distributions and three-dimensional flow patterns. Azad et al. (2000a) measured detailed tip surface heat transfer coefficient and pressure distributions of a turbine blade with a turning angle of 98° by using a transient liquid crystal technique. They found that for h/b = 1%, 1.5% and 2.5%, the tip clearance has a significant influence on local tip surface heat transfer distribution, and they identified different heat transfer regions on the tip surface. Rhee and Cho (2006a,b) reported local heat/mass transfer characteristics not only on the near-tip surface but also on the tip surface and shroud of a plane-tipped rotating blade for a fixed mean tip clearance-to-chord ratio of about 2.5% in a low-speed annular cascade for incidence angles ranging from −15° to 7°.

A full-length squealer tip provides an enclosed cavity over the turbine rotor blade tip surface. It is known that the squealer tip increases resistance to tip leakage to reduce the flow rate through the tip gap and protects the tip surface from full thermal impact of high temperature tip gap flow. Effects of cavity squealers on heat transfer were performed by Ameri et al. (1998) and by Azad et al. (2000b). Key and Arts (2006) compared plane tip leakage flow with cavity squealer tip one at high-speed conditions, and Lee and Chae (2008) investigated effects of cavity squealer rim height on aerodynamic losses. There are many other studies that deal with flow and/or heat transfer characteristics over various kinds of partial- and full-length (cavity) squealers such as a mean camberline strip (Ameri, 2001), a winglet squealer (Papa et al., 2003), single and double squealers (Kwak et al., 2003), various partial squealers (Heyes et al., 1992; Nasir et al., 2004; Newton et al., 2006), and single and channel-type squealers (Camci et al., 2005).

Even though there are many flow and heat transfer measurements over the various kinds of tips referred above, it is very hard to understand three-dimensional flow structure even within a plane tip gap with the variation of tip gap height. As far as the authors know, Fig. 1 suggested by Bindon (1989) seems to be the only flow sketch that describes a complete history of plane tip gap separation bubble. Although numerical visualizations within plane tip gaps were reported by Ameri and Bunker (2000), by Tallman and Lakshminarayana (2001), and by Newton et al. (2006), unfortunately, there are discrepancies among their flow structures especially near the leading edge.

In this study, the effects of tip gap height-to-chord ratio, h/c, on the three-dimensional flow structure and heat/mass transfer over the plane tip of a high-turning turbine rotor blade have been investigated experimentally. This paper is different from the previous measurements such as Yamamoto (1989), Bunker et al. (2000), Azad et al. (2000a), Rhee and Cho (2006b), and Newton et al. (2006), because its objectives are (i) to identify a pair of leading edge tip gap vortices and converging flows toward the mid-chord within a separation bubble, (ii) to understand how they behave with h/c from 1.0% to 4.0%, (iii) to understand how the tip gap flow phenomena influence local heat/mass transfer rate with h/c, and (iv) to propose new tip gap flow models for low and high tip gap heights.

In order to do these, for a large-scale turbine blade, which could provide a good spatial resolution particularly close to the tip edge, we employed not only a high-resolution oil film method to visualize the tip surface flow but also the naphthalene sublimation technique to measure tip surface heat/mass transfer rate without wall conduction error.

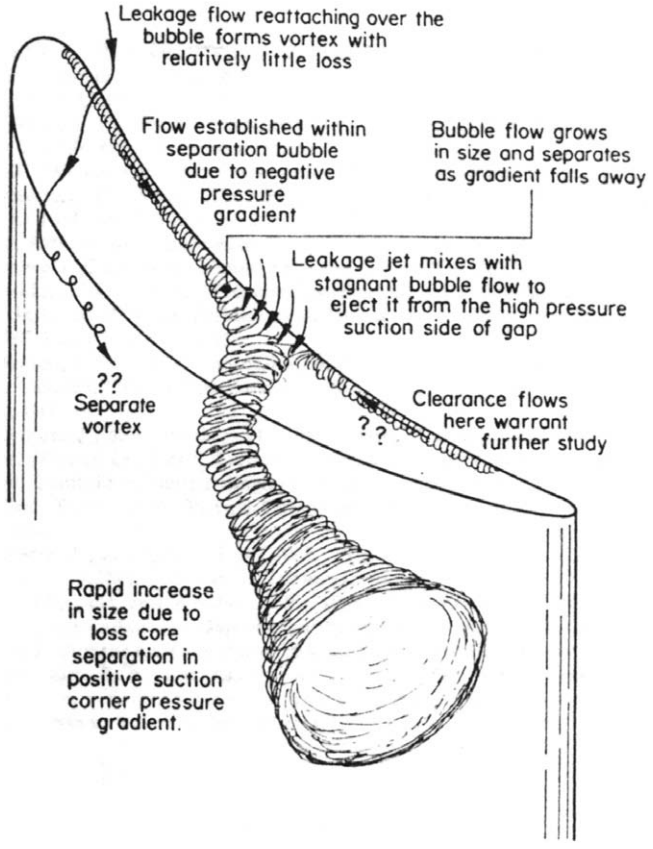

Fig. 1. A complete history of tip gap separation bubble suggested by Bindon (1989).

2. Experiment

2.1. Linear turbine cascade with tip gap

The cascade wind tunnel in Fig. 2 comprises an open-circuit type wind tunnel, an inlet duct, and a linear turbine cascade with tip clearance gap, and an exit duct. The inlet duct has a cross section of 0.42 m × 0.32 m. The flow coming out from the wind tunnel is developing to a turbulent boundary layer flow on the top and bottom walls of the inlet duct, after passing a trip wire of 1.8 mm in diameter and sand paper. As shown in Fig. 2, the turbine cascade has six linear turbine blades, and its entrance is located 1.20 m downstream of the wind tunnel exit. The exit duct has a tailboard to adjust periodicity among the blade passage flows.

The blades are fabricated in a large-scale based on the profile of a high-turning first-stage turbine rotor blade, and they are made of aluminum. As listed in Fig. 3, the chord, c, axial chord, b, pitch, p, and span, s, are 217.8 mm, 196.0 mm, 151.6 mm, and 320.0 mm, respectively. The span illustrated in Figs. 2 and 4 is based on aspect ratio of the original blade of $s/c = 1.47$. This rotor blade has a high turning angle of 119.0°. The blade profile used in this study is reported by Lee and Chae (2008). As in Fig. 2, the central four blades can be inserted into the indents machined on the bottom wall, and thus they have a tip gap height, h, on the top end (Fig. 4). On the other hand, the two far-end blades of #1 and #6 act as guide vanes with no tip gap. In the xyz coordinates, x, y, and z are in the axial, pitch-wise and span-wise directions of the cascade (Figs. 3 and 4).

2.2. Tip surface flow visualization

Due to very thin tip gap spaces, it is not easy to measure three-dimensional velocity fields directly within the tip gap. In this study, we employed a high-resolution oil film method using a mixture of fine carbon black powder and kerosene as in Lee et al. (2001). In order to videotape mixture movements, the top endwall is replaced by a transparent glass of 8.0 mm in thickness. Before each experiment, a white contact paper is attached on the tip surface and the mixture is spread evenly on the contact paper. During the visualization process, the tip surface is videotaped until kerosene is completely evaporated. Then, the contact paper is removed from the tip surface and is attached on a hard board. Finally, the visualization is coated with a transparent paint to prevent its spoil from contacts. The videotaped image provides valuable information on near-wall local flow directions.

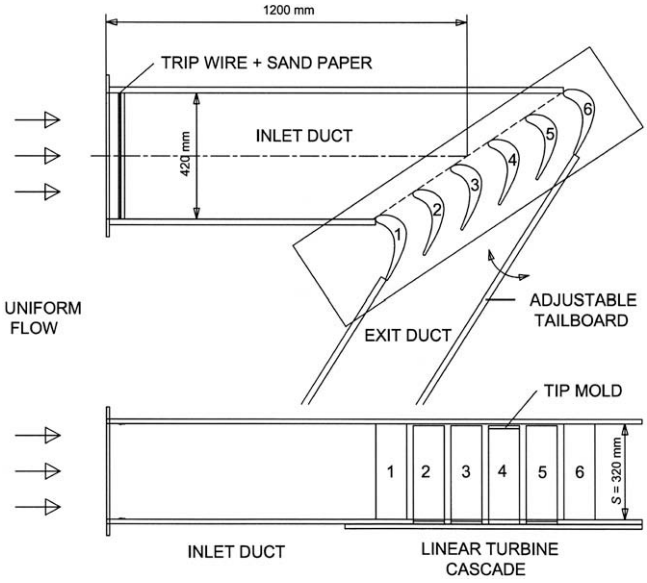

Fig. 2. Overall view of cascade wind tunnel with tip gap.

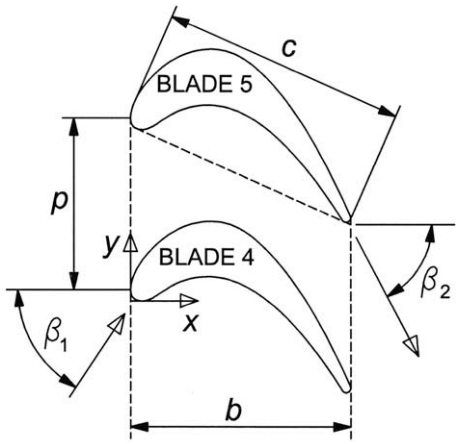

Number of blades	6
Chord length (c)	217.8 mm
Axial chord (b)	196.0 mm
Pitch (p)	151.6 mm
Span (s)	320.0 mm
Blade inlet angle (β_1)	56.4 deg
Blade outlet angle (β_2)	-62.6 deg

Fig. 3. Cascade data.

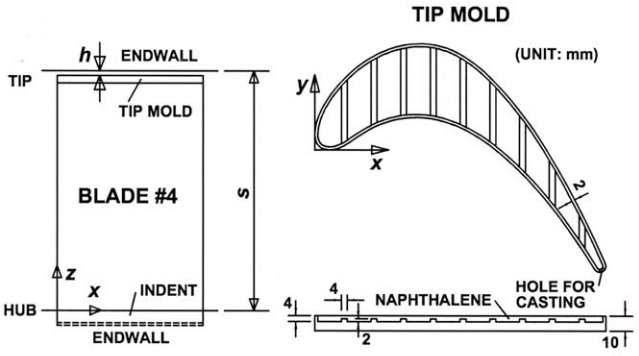

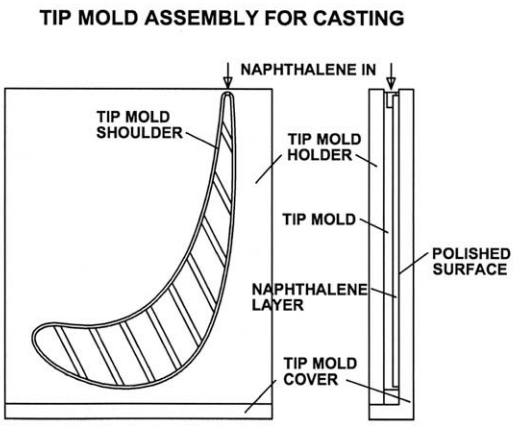

Fig. 4. Mold for naphthalene-coated tip surface.

2.3. Local heat/mass transfer rate measurements

2.3.1. Naphthalene sublimation technique

In this technique, mass transfer coefficient, h_m, is evaluated from the corresponding sublimation depth of cast naphthalene. Local Sherwood number, Sh, which is commonly used as a dimensionless mass transfer coefficient, is defined as:

$$\mathrm{Sh} = (h_m c)/D \tag{1}$$

where D is the diffusion coefficient of naphthalene in air. According to an analogy between heat and mass transfer (Goldstein and Cho, 1995), Nusselt number can be obtained in the following way:

$$\frac{\mathrm{Nu}}{\mathrm{Sh}} = \left(\frac{\mathrm{Pr}}{\mathrm{Sc}}\right)^n \tag{2}$$

where n is usually taken to be 1/3 for a laminar flow and to be 0.4 for a turbulent one. The boundary condition in the mass transfer system is equivalent to the constant surface temperature condition in the heat transfer system.

2.3.2. Naphthalene coated plane tip

A tip mold assembly for naphthalene casting is presented in Fig. 4. The tip mold assembly comprises a tip mold, a tip mold holder, and a cover with a polished surface. All of them are made of aluminum and are bolted together. The tip mold has a thickness of 10 mm and has a very narrow shoulder of 2 mm in width. A thin naphthalene layer of 4 mm in thickness is cast inside the grooved cavity between the tip mold and the polished cover surface. In order to minimize flow disturbances during wind tunnel tests, molten naphthalene is poured through a hole located on the trailing edge as shown in the tip mold assembly. A T-type thermocouple is embedded in the cast naphthalene through the hole to obtain the naphthalene surface temperature during the sublimation experiments. The cast plane tip mold is positioned on the top end of the blade #4 as in Figs. 2 and 4.

2.3.3. Data reduction system and procedure

The measurements of velocity, turbulence, temperature and naphthalene sublimation depth are controlled by a personal computer (IBM, Pentium 4) equipped with plug-in boards such as a Multi-Function DI/O Board (NI, PCI-MIO-16E-4) and a GPIB adapter (NI, AT-GPIB). Velocities are measured with a micro-monometer (MKS, 223BD-00010ACB). Temperatures of the free-stream and the cast naphthalene are measured with T-type thermocouples connected to a digital voltmeter (Keithley, Model 2001TSCAN), which is controlled by the computer through the GPIB. The thermocouples are calibrated using a constant-temperature bath (Fisher Scientific, 9010) and a standard thermometer. The temperature measurements are based on the STP 470A (1974) published by ASTM.

A LVDT (linear variable differential transformer) depth gauge (Sensortec, 060-3590-02) is used to measure local sublimation depth (Lee et al., 2004). Its full scale and resolution are ±1.0 mm and 1.0 μm, respectively. Sublimed depth is measured at 50 points in the x-direction and at 15 points in the y-direction as shown in Fig. 5. The measurement locations are populated densely in the leading and trailing edge regions as well as near the tip edge.

When a smooth tip surface of naphthalene is obtained from the cast procedure, the test tip mold is mounted on a profile measuring system, and the first scanning of the naphthalene surface is conducted with the calibrated depth gauge at the 750 locations, before exposure to the air flow. It takes about 15 min to complete the total scanning. The readings of local elevation are recorded in the computer through the 12-bit A-D converter. Then, the cast tip mold is positioned in the cascade as in Fig. 2. After it is exposed to the air flow, it is brought back to the profile measuring system, and is scanned again. The difference between the before-and-after readings at each location still includes free convection loss during the setup time of the cast tip mold as well as during the depth measurements. The net sublimation depth is finally obtained after a proper correction.

2.4. Operating conditions and uncertainties

During all the experiments, the free-stream velocity measured 1.5c upstream of the cascade inlet is maintained at U_∞ = 15 m/s. A good pitch-wise mean flow periodicity is obtained at the entrance of the central three blade passages within 2% deviation.

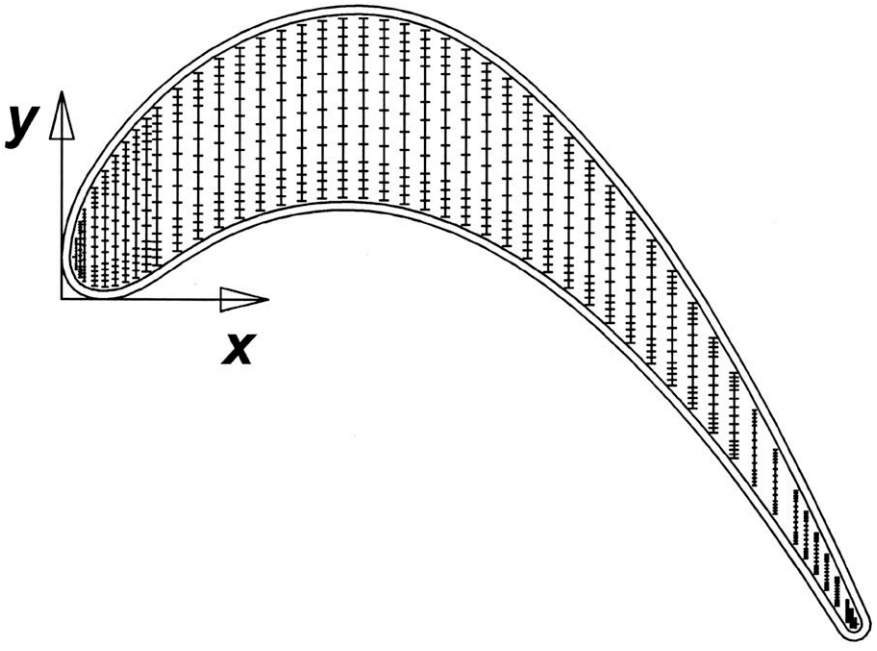

Fig. 5. Sublimation depth measurement locations.

The inlet Reynolds number based on the free-stream velocity and the chord, Re_{∞}, is 2.09×10^5. The inlet turbulence intensity 1.5c upstream of the cascade entrance is 0.3%, and the boundary layer thickness, displacement thickness, and momentum thickness measured on the top wall are 44.7 mm, 5.16 mm, and 4.04 mm, respectively. In this study, the tip gap-to-chord ratio is changed to be h/c = 1.0%, 2.0%, 3.0% and 4.0% which correspond to h/s = 0.68%, 1.36%, 2.04% and 2.72%, respectively. The static-pressure coefficients along the blade pressure and suction surfaces at the mid-span with no tip gap are reported by Lee and Chae (2008). During exposure of cast naphthalene to the cascade air flow, its surface temperature is kept within 0.2 °C. The uncertainty interval of Sh with 95% confidence based on Abernethy et al. (1985) is estimated to be ±5.7% of Sh.

3. Results and discussion

3.1. Two distinct flow phenomena within the tip gap

In this study, two major flow phenomena, a pair of vortices found in the leading edge region and a flow separation/re-attachment process over the pressure-side tip edge, are identified based on the tip surface flow visualizations. The relative importance of the two phenomena characterizes the overall tip gap flow structure.

3.1.1. Tip gap vortices

A magnified oil film flow visualization in the leading edge region for h/c = 3.0% is shown in Fig. 6. The C-shaped dash-dot line is a locus of local peak heat/mass transfer rate drawn from the present data introduced later in Fig. 10c. The dotted ellipse upstream of the dash-dot line represents the boundary of an area where oil film mixture accumulates. Therefore, the area is covered with a thin carbon black layer after evaporation of its kerosene. There exists a C-shaped darker area downstream of the dash-dot line, and a C-shaped brighter area with clear imprints of near-wall flow direction is observed just upstream of the dash-dot line. The darker area is resulted from the lower near-wall momentum in parallel with the tip surface as indicated in Fig. 7. The arrows in the brighter area in Fig. 6 are drawn from the local oil film traces and show the local near-wall flow directions which are also confirmed from the videotaped mixture movements.

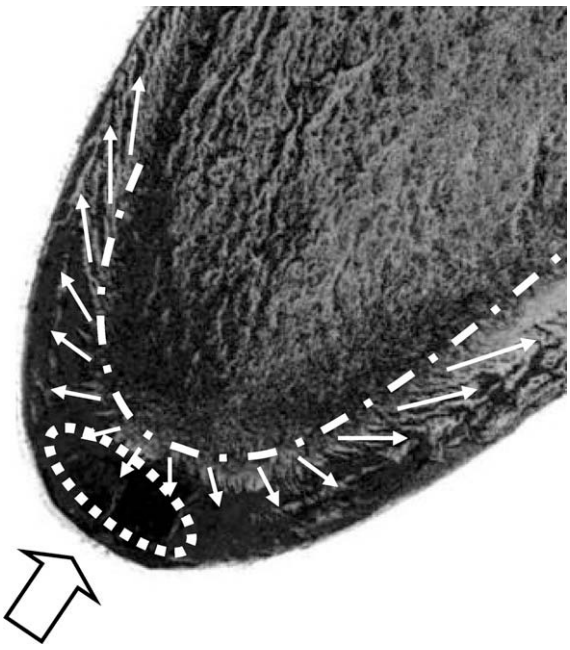

Fig. 6. Leading edge tip surface flow visualization for h/c = 3.0%.

The leading edge flow features in Fig. 6 strongly suggest that there exists a rolling-up of fluid separated over the tip edge, as shown in Fig. 7, and it is converted into a pair of vortices in the opposite directions along the dash-dot line. In this study, these vortices are named "tip gap vortices". The tip gap vortices developing along the pressure- and suction-side tip edges correspond to the pressure- and suction-side tip gap vortices, respectively.

The separated fluid over the tip edge would be influenced not only by the shearing of neighboring near-tip main passage flow moving along the convex surface of the leading edge but also by the favorable pressure gradient from the stagnation plane to a downstream location along the dash-dot line. Both of them tend to stimulate flow divergence away from the stagnation plane, which leads to three-dimensional spiral flows in the opposite directions. These are why the tip gap vortices are generated within the tip gap near the leading edge.

Fig. 7 presents a schematic flow sketch for h/c = 3.0% in the stagnation plane of on-coming flow entering the tip gap. The tip gap height, the length of the mixture accumulation, and the location of local peak heat/mass transfer rate are scaled based on the measured dimensions. In the stagnation plane, fluid approaching the tip gap inlet is separated over the tip edge and rolls up to form a pair of vortices. The reverse flow existing between the assumed vortex center and the tip surface pushes oil film mixture in the upstream direction, which results in mixture accumulation, as in the dotted area in Fig. 6. Just downstream of the dash-dot line, near-wall momentum parallel to the tip surface is not so high. This is why there exists the darker area as mentioned above.

3.1.2. Flow separation/re-attachment

Fig. 8 shows a typical flow separation/re-attachment phenomenon on the tip surface in the mid-chord region for h/c = 3.0%. The dash-dot line drawn based on a locus of local peak heat/mass transfer rate is considered as a re-attachment line. The imprinted flow patterns and videotaped mixture movements show that near-wall flow is divided clearly by the dash-dot line. On-coming fluid separated over the upstream pressure-side tip edge re-attaches to the tip surface along the dash-dot line. Then most of it moves toward the suction-side as indicated by the long arrows meanwhile the remainder flows back as shown by the short arrows within the separation bubble. In addition, there exists a flow converging area in the mid-chord region bounded by the dotted ellipse in which oil film mixture accumulates. Near-wall fluid within the separation bubble has a tendency to move toward this flow converging area, due to the strong concave curvature of the present high-turning blade at the mid-span. This flow phenomenon will be discussed in detail in Fig. 9 with the variation of h/c.

None of the previous experimental and numerical investigations reported distinct evidences for the existence of the tip gap vortices and the flow convergence toward the mid-chord. Only the CFX numerical flow visualizations by Newton et al. (2006) reported the leading edge tip gap flow similar to the present one.

3.2. Effect of tip gap height on tip surface flow

Surface flow visualizations for tip gap height-to-chord ratios of h/c = 1.0%, 2.0%, 3.0%, and 4.0% are reported in Fig. 9. The blank arrow near the leading edge in each visualization indicates on-coming flow direction, and the dash-dot line represents a locus of local peak heat/mass transfer rate based on the results in Fig. 10. It is revealed from Fig. 9 that two typical flow phenomena, tip gap vortices and a flow separation/re-attachment process, depend strongly on h/c.

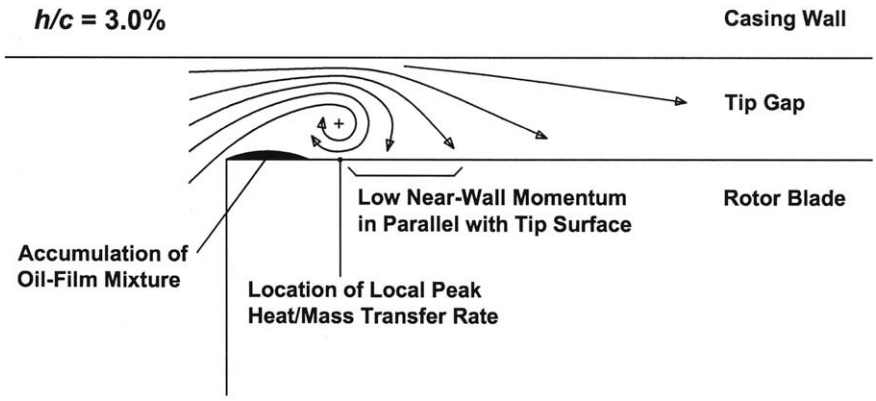

Fig. 7. Flow sketch near the leading edge in the stagnation plane for $h/c = 3.0\%$.

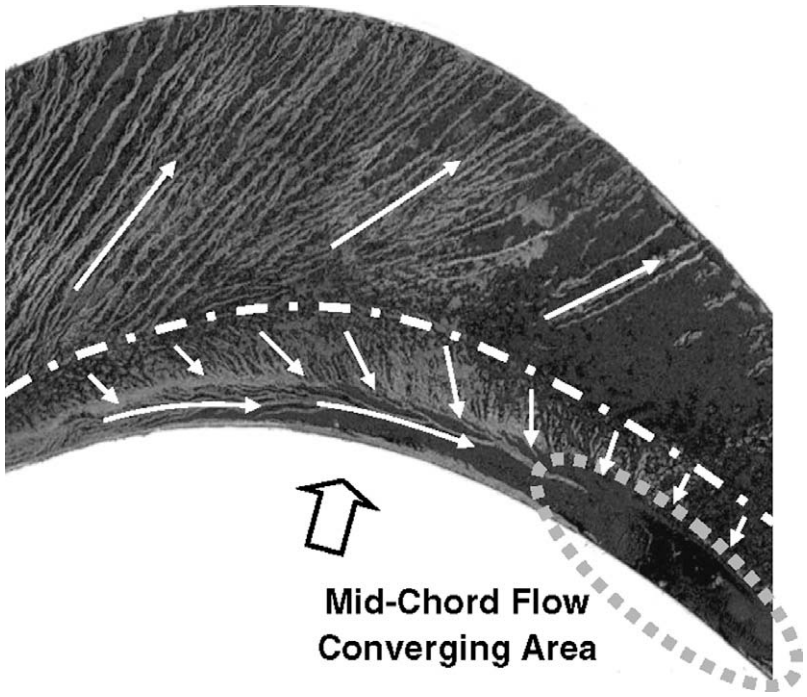

Fig. 8. Mid-chord tip surface flow visualization for $h/c = 3.0\%$.

3.2.1. Tip gap vortices

A close examination of the flow patterns in the case of $h/c = 1.0\%$ (Fig. 9a) shows that there are no evidences for the existence of the tip gap vortices such as a C-shaped darker area, a C-shaped brighter area with clear imprints of flow direction, and an area where oil film mixture accumulates, as discussed earlier in Fig. 6. When $h/c \geqslant 2.0\%$, however, a pair of tip gap vortices can be identified, because all the evidences are found clearly in Fig. 9b–d. Local tangential lines of flow traces along the dash-dot line are in parallel with it in the region upstream of the mid-chord especially for wider tip gaps such as $h/c = 3.0$ and 4.0%, which means that near-wall flow along the dash-dot line has a large velocity component tangent to it. This implies that the pressure-side tip gap vortex would develop in parallel with the re-attachment line. Between the mid-chord and the trailing edge, however, flow traces near the dash-dot line appear to be normal to it.

3.2.2. Re-attachment line

In the case of $h/c = 1.0\%$, the dash-dot line cannot be identified in the leading edge region, because it seems to be located very close to the upstream tip edge out of the present mass transfer measurement area. With increasing h/c, the dash-dot re-attachment line recedes farther away from the upstream tip edge line, and flow patterns within the separation bubble become more complicated. In the widest tip gap case of $h/c = 4.0\%$, the dash-dot line is broken into two lines at last. The dipper-shaped one located closer to the leading edge is considered as a centerline of the tip gap vortices. The other one found between the mid-chord and the trailing edge is located far away from the upstream tip edge, as a result of strong flow separation/re-attachment.

3.2.3. Mid-chord flow converging area

In the lowest h/c case (Fig. 9a), on-coming flow into the tip gap inlet re-attaches to the tip surface immediately after separation over the upstream tip edge, so that the separation bubble is found very short. There are no complicated near-wall flow traces converging toward the mid-chord within the separation bubble. In the case of $h/c = 2.0\%$, however, there begins to exist the mid-chord flow converging area enclosed by the dotted ellipse. Oil film mixture within the separation bubble moves toward it from the

trailing edge as well as from the leading edge, as indicated by the two arrows in the opposite directions in Fig. 9b. With the increment of h/c, the separation bubble becomes longer (and higher) near the flow converging area, which would serve as a flow resistance. This is why a dark area with almost no flow traces, where near-wall flow is nearly stagnant, is found downstream of the flow converging area for h/c = 3.0% and 4.0%. Lower near-wall momentum in these dark areas in Fig. 9c and d would deliver lower convective transport. It is interesting from Fig. 9c and d that even if the separation bubble is long enough, the flow moving toward the mid-chord is confined to a very narrow area adjacent to the upstream tip edge. Flow within the separation bubble is found most complicated and most three-dimensional in the widest tip gap case in Fig. 9d.

3.2.4. Flow direction near the downstream tip edge

The flow visualizations also show that in the case of h/c = 1.0%, flow directions near the downstream suction-side tip edge line are skew with respect to it near the leading edge and in the region from the mid-chord to the trailing edge, but they are approximately normal to it in the region between the leading edge and the mid-chord. With increasing h/c, however, flow directions become skew even in the mid-chord region.

3.3. Distributions of Sherwood number

Contours of Sh on the plane tip surface are presented in Fig. 10 for h/c = 1.0%, 2.0%, 3.0% and 4.0%. The tip surface can be divided into four regions based on the local heat/mass transfer data in Fig. 10. Region A is a lower heat/mass transfer area near the suction-side, Region B is a higher heat/mass transfer area resulted from flow re-attachment, Region C is a higher heat/mass transfer area along the tip gap vortices, and Region D is a lower heat/mass transfer area identified near the mid-chord flow converging area. In general, the location and occupation area of each region are strongly dependent upon h/c.

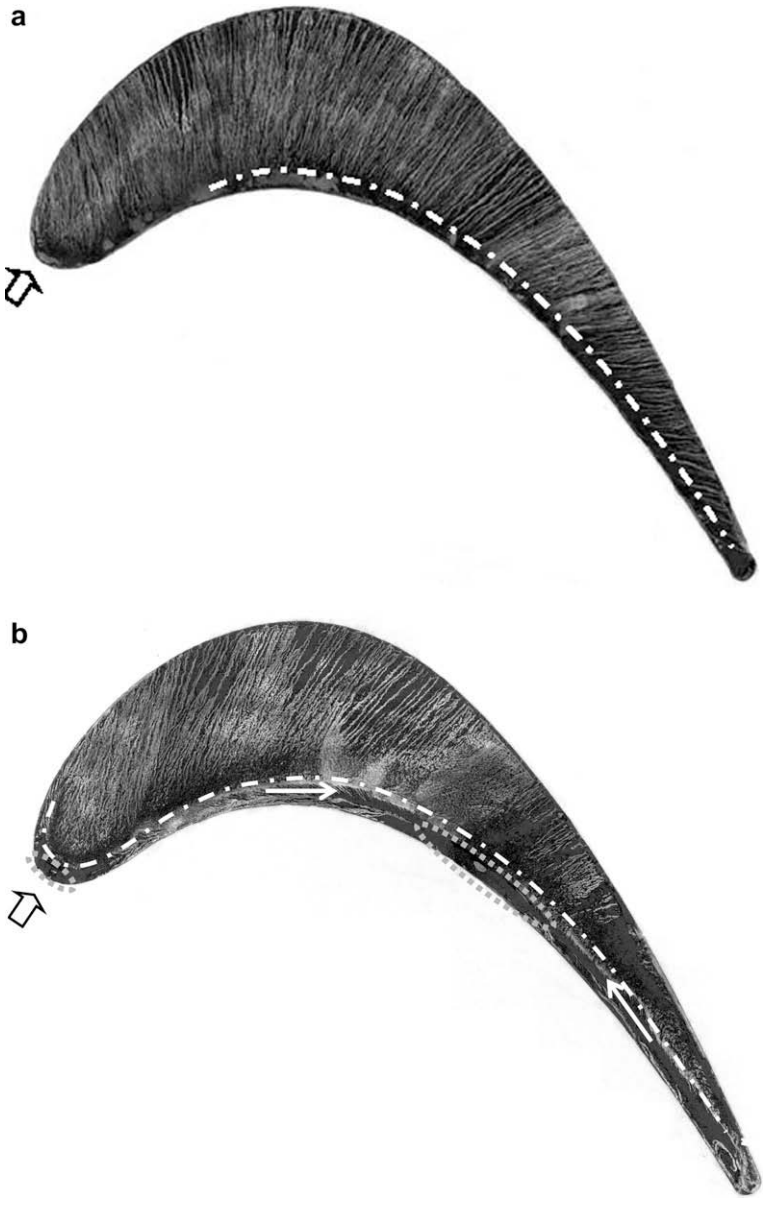

Fig. 9. Tip surface flow visualizations. (a) h/c = 1.0%; (b) h/c = 2.0%; (c) h/c = 3.0%; (d) h/c = 4.0%.

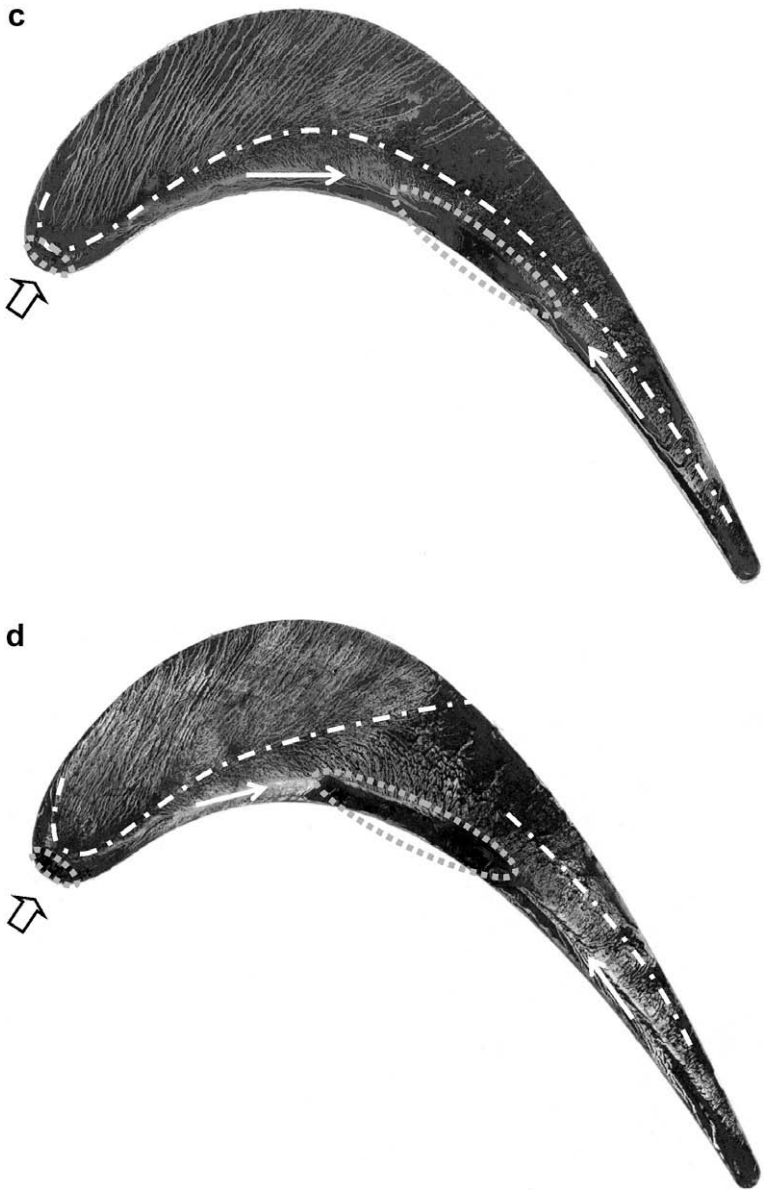

Fig. 9 (*continued*)

In the case of h/c = 1.0% (Fig. 10a), higher Sh with its steep gradient is always found near the upstream tip edge and its maximum value is found at the mid-chord in Region B and is higher than 4800. This is because on-coming flow is separated over the upstream tip edge, and then it re-attaches to the tip surface shortly. Therefore, the re-attachment line, a locus of local peak Sh, is nearly in parallel with the upstream tip edge line, slightly away from it. In this narrow tip gap case, each contour is found in parallel with the upstream tip edge line, which implies that there is a two-dimensional flow with little flow change in the chord-wise direction. In this case, Region A has a relatively wide area in the downstream region along the suction-side tip edge line due to thick boundary layer, but it is hard to identify Region C from Region B because no vortices are found near the leading edge. It is not easy to find Region D near the pressure-side edge.

As h/c increases from 1.0% to 2.0%, the re-attachment line advances farther in the downstream direction and Sh along it tends to decrease with less severe Sh gradient. Examining the magnified plot in Fig. 10b, each contour in the leading edge region is in the form of a thin crescent in contrast to a round curve in parallel with the tip edge line for h/c = 1.0% (Fig. 10a). For h/c = 1.0%, the local peak value of Sh near the leading edge is found along the boundary of the present measurement area. For h/c = 2.0%, however, its C-shaped locus, which is considered as a vortex centerline, is found slightly away from the measurement boundary. These facts assure that for h/c = 2.0%, there exists not only a rolling-up of on-coming separated flow but also a pair of tip gap vortices. For h/c = 2.0%, it is possible to identify Region C from Region B near the leading edge. The boundary between the two region is located at about x/b = 0.17, and thus this Region C is much shorter than Region B. Region A has a smaller area behind the tip gap vortex system in comparison with that in the case of h/c = 1.0%. On-coming fluid entering the tip gap near the leading edge is separated over the sharp tip edge and then some portion of the separated fluid turns back near the tip surface as illustrated in Fig. 7. This flow reversal continues to happen along the pressure- and suction-side tip edge

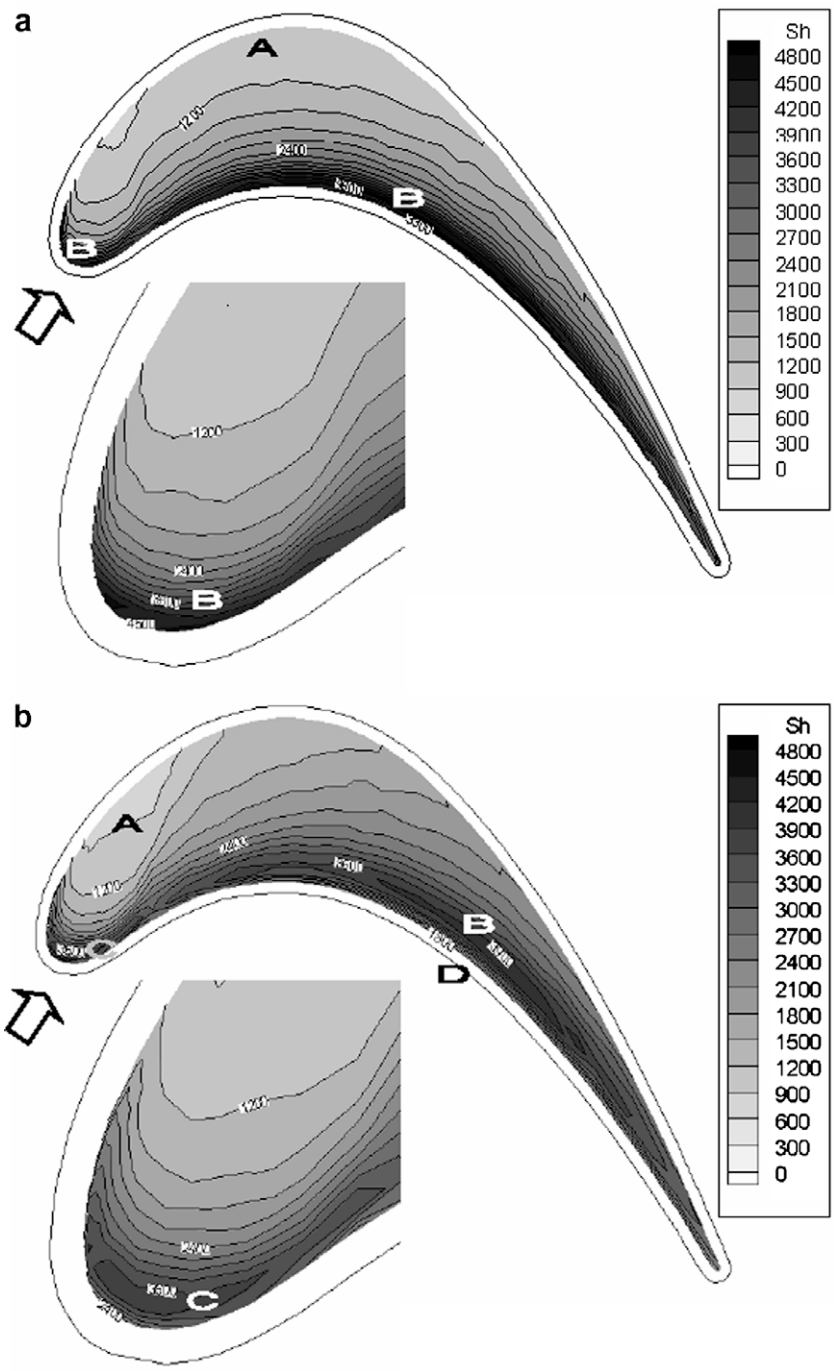

Fig. 10. Contours of Sherwood number. (a) h/c = 1.0%; (b) h/c = 2.0%; (c) h/c = 3.0%; (d) h/c = 4.0%.

line off the stagnation plane as in Fig. 6, to form the tip gap vortices. As a result, the mass flow rate behind the tip gap vortices seems to be low enough, which results in lower convective heat/mass transfer rate in Region A. This Region A is also found by Bunker et al. (2000) as the "sweet spot", by Azad et al. (2000a), and by Newton et al. (2006), but their explanations for its existence are somewhat different from the present one. These previous heat transfer data seem to fail to provide the crescent-shaped contours near the leading edge probably due to wall conduction error. Mass transfer measurement by Rhee and Cho (2006a,b) did not show these crescent-shaped ones due to the thick shoulder of their tip mold. In this case of h/c = 2.0%, Sh near the pressure-side edge line has a value of about 1800 in Region D, which is much lower than that of about 3300 for h/c = 1.0%. The presence of Region D at the mid-chord supports the existence of the mid-chord flow converging area.

In the case of h/c = 3.0% (Fig. 10c), overall heat/mass transfer distribution has the same trend as that for h/c = 2.0%, in general. In this case, many contours away from the upstream tip edge are not parallel with it any more. This fact means that the tip gap flow has a three-dimensional nature. The crescent-shaped contours in the magnified plot in Fig. 10c also demonstrate the presence of a pair of tip gap vortices. Region C occupied by the tip gap vortices extends from the leading edge up to around x/b = 0.5, and is even wider than that for h/c = 2.0%.

These heat/mass transfer characteristics are much deepened in the case of h/c = 4.0% (Fig. 10d). The most important feature in this widest tip gap case is an extension of Region C up to the mid-chord

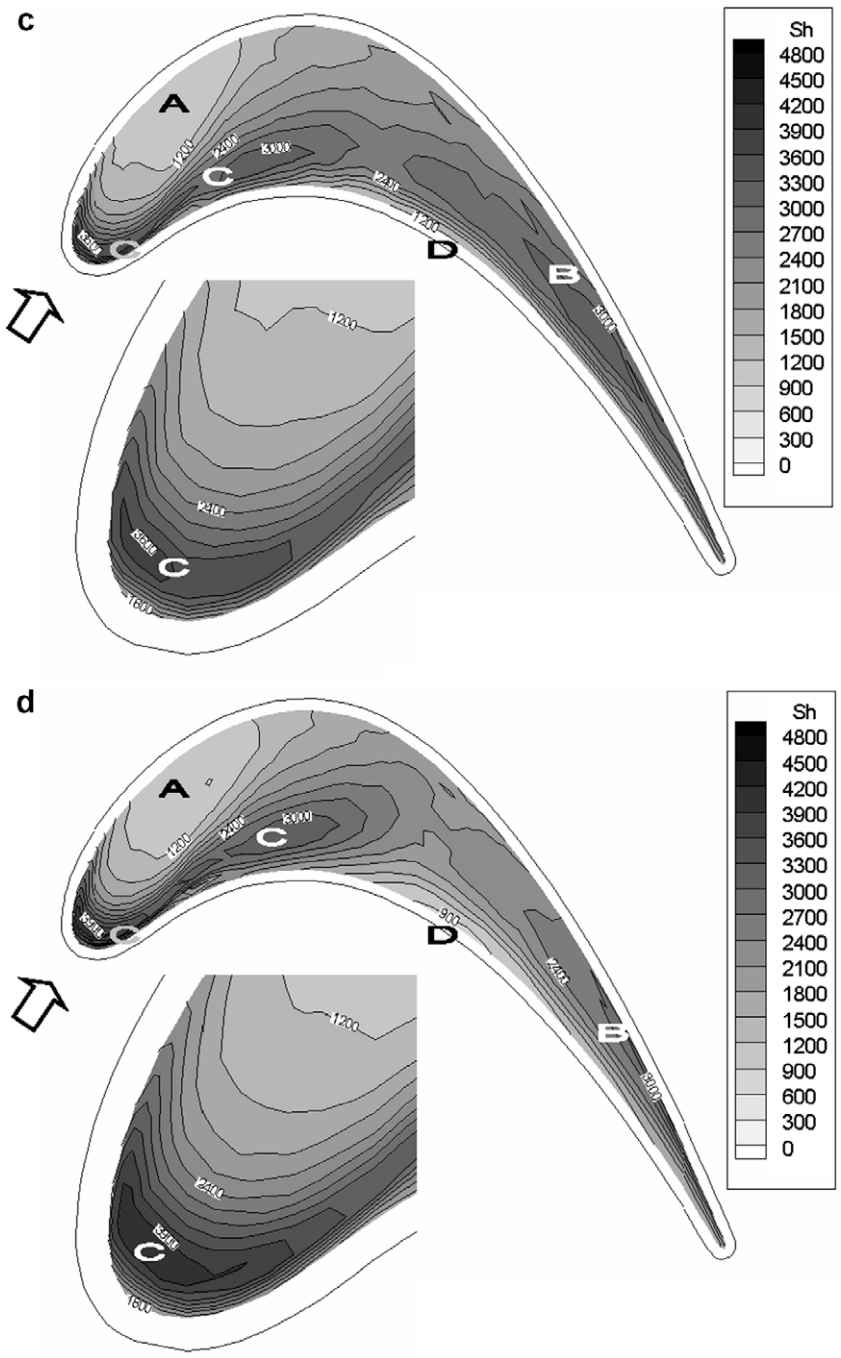

Fig. 10 (*continued*)

suction-side tip edge, which delivers a break-up of the dash-dot line into two parts as shown in Fig. 9d. It is noted that in this widest tip gap case, Sh found in Region D at the mid-chord is as low as about 900.

It is very interesting that Sh along its peak locus has a local maximum at the mid-chord when $h/c \leqslant 2.0\%$, but it has a local minimum in the mid-chord region when $h/c \geqslant 3.0\%$. This is probably because flow separated over the mid-chord upstream tip edge for lower h/c has higher local mass flow rate due to the mid-chord concave curvature, meanwhile that for higher h/c has lower local mass flow rate due to the increment of flow resistance arising from the longer and higher mid-chord flow converging area. The presence of a dark area with almost no flow traces downstream of the mid-chord converging area in Fig. 9c and d supports this theory.

The loci of local peak Sh are presented in Fig. 11 with the variation of h/c. With increasing h/c, the locus advances toward the suction-side and is finally broken into two parts in the case of $h/c = 4.0\%$. As h/c increases, the C-shaped locus near the leading edge moves away from the round tip edge, which implies that wider tip gap leads to stronger rolling-up of separated fluid and then to more intensified tip gap vortices in turn. Particularly when h/c increases from 3.0% to 4.0%, however, the advancement of the locus near the leading edge is found minute.

In summary, the present heat/mass transfer data strongly support the existence of the tip gap vortices, the flow separation/re-

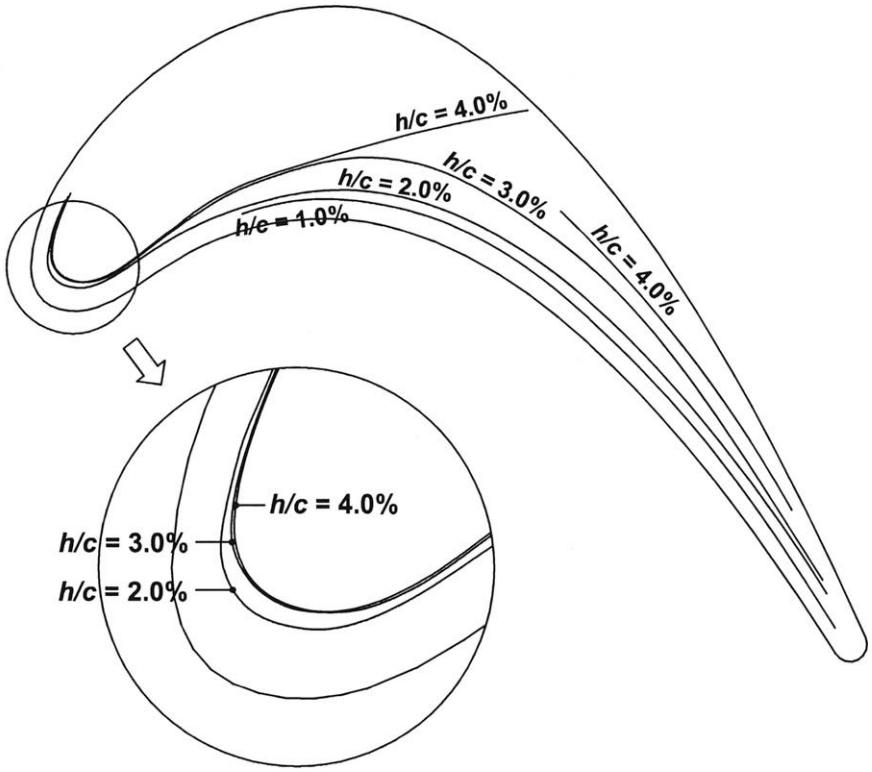

Fig. 11. Loci of local peak heat/mass transfer rate with the variation of *h*/*c*.

attachment, and the mid-chord flow converging area. With the increment of *h*/*c* from 1.0% to 4.0%, Region A in the form of a long strip near the suction-side becomes a small area behind of the tip gap vortex system, and Region B shifts from the location very close to the pressure-side tip edge to that near the suction-side between the mid-chord and the trailing edge. Region C begins to exist in a crescent-shaped narrow region near the leading edge for *h*/*c* = 2.0%, and then extends up to the suction-side tip edge for *h*/*c* = 4.0%. Region D is identified near the mid-chord converging area. With the increment of *h*/*c* from 2.0% to 4.0%, local minimum Sh in Region D tends to decrease. At last, Sh in the case of *h*/*c* = 4.0% has its lowest value not in Region A but in Region D, contrary to the other cases.

3.4. Tip gap flow models

Based on the present surface flow visualizations and heat/mass transfer data, new realistic flow models have been proposed for *h*/*c* = 1.0% and 4.0% as in Fig. 12a and b. In these figures, the boundaries of Region A and Region D are drawn based on local contours of Sh = 1200, and those of Region B and Region C are equivalent to local contours of Sh = 2400. The arrow with its solid head denotes a local near-wall flow direction obtained from the surface flow traces in Fig. 9a and d, and the blank-head arrow in Fig. 12b indicates an expected local upward flow direction in the mid-chord flow converging area.

3.4.1. Tip gap flow model for h/c = 1.0%

When *h*/*c* = 1.0% (Fig. 12a), on-coming fluid which approaches the tip gap inlet is separated over the upstream tip edge, and then re-attaches immediately to the tip surface, so that the re-attachment line is very close to the upstream tip edge line. After the re-attachment, a boundary layer develops over the tip surface in the direction indicated by the arrows in Fig. 12a. In this low *h*/*c* case, there would be no considerable flow change in the chord-wise direction, and thus the tip gap flow is generally considered two-dimensional. Even though flow directions are skew with respect to the re-attachment line near the leading and trailing edges, there are no appreciable complicated three-dimensional flow phenomena such as tip gap vortices, and converging flows toward the mid-chord within the separation bubble. It is summarized in this low *h*/*c* case that the tip gap flow is dominated only by the flow separation/immediate re-attachment and the subsequent gradual boundary layer development.

3.4.2. Tip gap flow model for h/c = 4.0%

When *h*/*c* = 4.0% (Fig. 12b), the tip gap flow becomes fully three-dimensional and is governed by the two major flow phenomena: the formation of tip gap vortices and their development; and the strong flow separation/re-attachment process. In this wide tip gap case, there exists a rolling-up of on-coming fluid separated over the round tip edge, and it is converted into a pair of tip gap vortices. The suction-side tip gap vortex comes out of the tip gap soon, and then it migrates downward over the blade suction surface as shown by the dotted lines. This vortex trace over the suction surface is clearly observed in the heat/mass transfer distributions measured by Kwon and Lee (2006) and by Rhee and Cho (2006a), and is also found in the heat transfer data measured by Newton et al. (2006). The pressure-side tip gap vortex would develop in parallel with the pressure-side tip edge line and might be intensified with the aids of the added mass and momentum fed by the fluid separated over the adjacent tip edge. Judging from the heat/mass transfer data introduced in Fig. 10d, its intensity and occupation area are much stronger and wider than those of the suction-side tip gap vortex, respectively. This pressure-side tip gap vortex crosses the mid-chord region, and finally comes out of the tip gap. CFX numerical visualizations by Newton et al. (2006) support these subsequent developments of the pressure- and suction-side tip gap vortices.

In this high *h*/*c* case, the re-attachment line recedes farther away from the upstream tip edge in comparison with that in

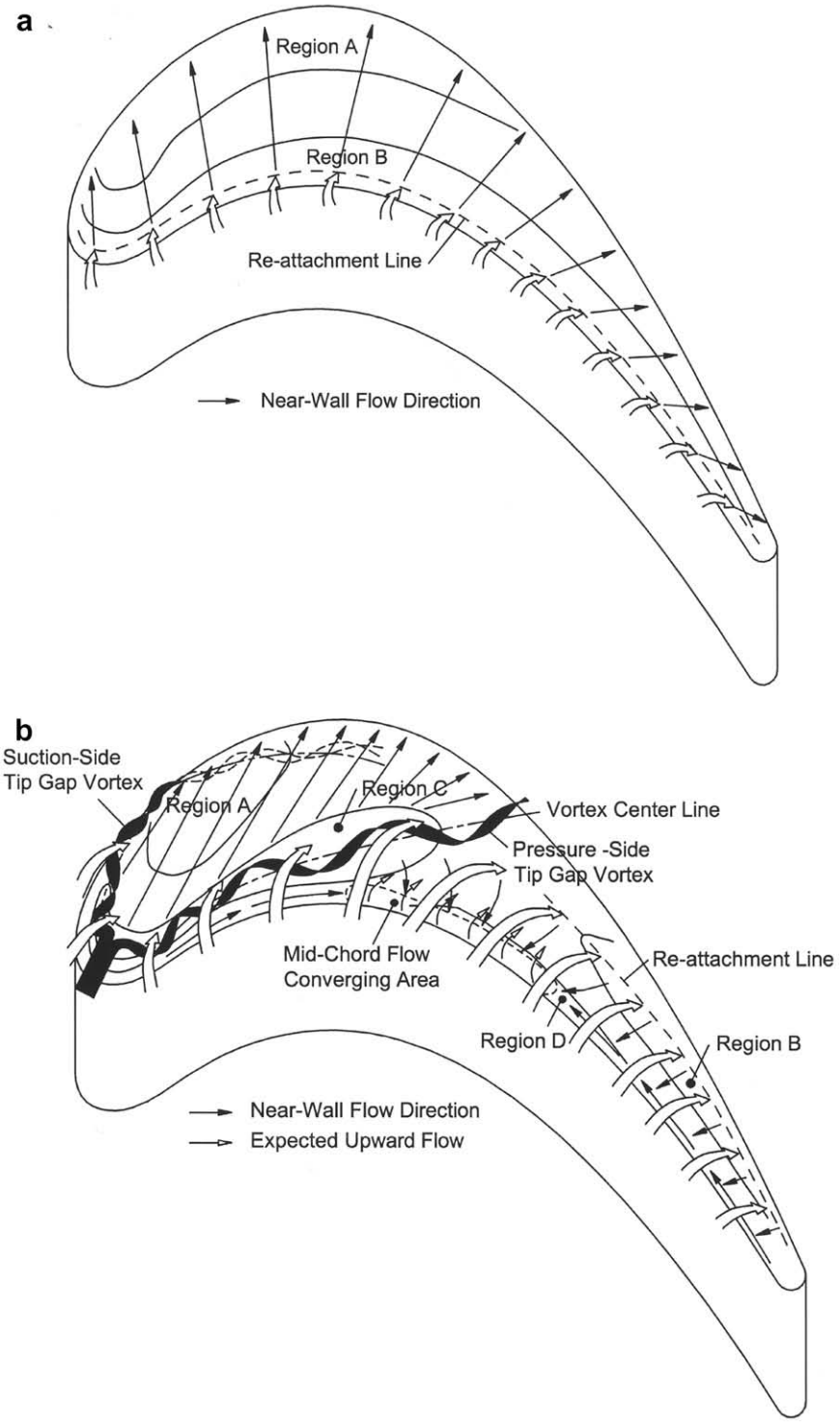

Fig. 12. Tip gap flow models over a plane tip. (a) $h/c = 1.0\%$; (b) $h/c = 4.0\%$.

Fig. 12a, and near-wall fluid within the separation bubble moves toward the mid-chord flow converging area not only from the leading edge but also even from the trailing edge. In this area, flow might be re-circulated, or might have a momentum away from the tip surface to be incorporated into the on-coming separated flow again as designated by the blank-head arrows in Fig. 12b. Bindon (1989) also suggested the flow convergence within the separation bubble toward the mid-chord as in Fig. 1, even though the flow from the trailing edge to the mid-chord was not assured yet. High turning angle of the present blade would expedite the flow convergence toward the mid-chord and the mid-chord break-up of the locus of local peak heat/mass transfer rate.

4. Conclusion

The effects of tip gap height-to-chord ratio, h/c, on the flow structure and heat/mass transfer over the plane tip surface of a high-turning turbine rotor blade have been investigated for

h/c = 1.0%, 2.0%, 3.0% and 4.0%, by using the high-resolution oil film method and naphthalene sublimation technique. The major findings in this study are summarized as follows.

(1) From the tip surface visualizations, a pair of vortices is identified in the leading edge region within the tip gap, and is named as "tip gap vortices", which tend to be intensified with increasing h/c.
(2) The tip gap flow is characterized by two major flow phenomena: the formation of the tip gap vortices and their subsequent developments; and the flow separation/re-attachment along the upstream tip edge line. The relative importance of the two flow phenomena depends strongly on h/c.
(3) Within the separation bubble, there exist complicated near-wall flows moving toward a mid-chord flow converging area not only from the leading edge but also from the trailing edge. With the increment of h/c, these converging flows toward it are strengthened with the enlargement of separation bubble.
(4) In general, higher thermal load is found along the loci of the tip gap vortices and along the re-attachment line, while lower thermal load is observed behind the tip gap vortex system and near the mid-chord flow converging area.
(5) Heat/mass transfer characteristics with the variation of h/c are discussed in detail in conjunction with the above-mentioned tip gap flow features.
(6) Based on the present flow visualizations and heat/mass transfer data, new realistic tip gap flow models have been proposed for h/c = 1.0% and 4.0%.

References

Abernethy, R.B., Benedict, R.P., Dowdell, R.B., 1985. ASME measurement uncertainty. Journal of Fluids Engineering 107, 161–164.

Ameri, A.A., 2001. Heat transfer and flow on the blade tip of a gas turbine equipped with a mean camberline strip. Journal of Turbomachinery 123, 704–708.

Ameri, A.A., Bunker, R.S., 2000. Heat transfer and flow on the first-stage blade tip of a power generation gas turbine: part 2-simulation results. Journal of Turbomachinery 122, 272–277.

Ameri, A.A., Steinthorsson, E., Rigby, D.L., 1998. Effect of squealer tip on rotor heat transfer and efficiency. Journal of Turbomachinery 120, 753–759.

Ameri, A.A., Steinthorsson, E., Rigby, D.L., 1999. Effect of tip clearance and casing recess on heat transfer and stage efficiency in axial turbines. Journal of Turbomachinery 121, 683–693.

Azad, Gm.S., Han, J.C., Teng, S., 2000a. Heat transfer and pressure distributions on a gas turbine blade tip. Journal of Turbomachinery 122, 717–724.

Azad, Gm.S., Han, J.C., Boyle, R.J., 2000b. Heat transfer and flow on the squealer tip of a gas turbine blade. Journal of Turbomachinery 122, 725–732.

Bindon, J.P., 1989. The measurement and formation of tip clearance loss. Journal of Turbomachinery 111, 257–263.

Bindon, J.P., Morphis, G., 1992. The development of axial turbine leakage loss for two profiled tip geometries using linear cascade data. Journal of Turbomachinery 114, 198–203.

Bunker, R.S., Bailey, J.C., Ameri, A.A., 2000. Heat transfer and flow on the first-stage blade tip of a power generation gas turbine: part 1-experimental results. Journal of Turbomachinery 122, 263–271.

Camci, C., Dey, D., Kavurmacioglu, L., 2005. Aerodynamics of tip leakage flows near partial squealer rims in an axial flow turbine stage. Journal of Turbomachinery 127, 14–24.

Chyu, M.K., Moon, H.K., Metzger, D.E., 1989. Heat transfer in the tip region of grooved turbine blades. Journal of Turbomachinery 111, 131–138.

Goldstein, R.J., Cho, H.H., 1995. A review of mass transfer measurements using naphthalene sublimation. Experimental Thermal and Fluid Science 10, 416–434.

Heyes, F.J.G., Hodson, H.P., Dailey, G.M., 1992. The effect of blade tip geometry on the tip leakage flow in axial turbine cascades. Journal of Turbomachinery 114, 643–651.

Key, N., Arts, T., 2006. Comparison of turbine tip leakage flow for flat tip and squealer tip geometries at high speed conditions. Journal of Turbomachinery 128, 213–220.

Kwak, J.S., Ahn, J., Han, J.C., Lee, C.P., Bunker, R.S., Boyle, R., Gaugler, R., 2003. Heat transfer coefficients on the squealer tip and near-tip regions of a gas turbine blade with single or double squealer. Journal of Turbomachinery 125, 778–789.

Kwon, H.G., Lee, S.W., 2006. Heat/mass transfer characteristics in the near-tip region on a turbine blade surface under combustor-level high inlet turbulence. Journal of Mechanical Science and Technology 21, 486–494.

Lee, S.W., Chae, B.J., 2008. Effects of squealer rim height on aerodynamic losses downstream of a high-turning turbine rotor blade. Experimental Thermal and Fluid Science 32, 1440–1447.

Lee, S.W., Park, S.W., Lee, J.S., 2001. Flow characteristics inside circular injection holes normally oriented to the crossflow: part I – flow visualizations and flow data in the symmetry plane. Journal of Turbomachinery 123, 266–273.

Lee, S.W., Jun, S.B., Park, B.K., Lee, J.S., 2004. Effects of combustor-level inlet turbulence on the endwall flow and heat/mass transfer of a high-turning rotor cascade. Journal of Mechanical Science and Technology 18, 1435–1450.

Metzger, D.E., Rued, K., 1989. The influence of turbine clearance gap leakage on passage velocity and heat transfer near blade tips: part I-sink flow effects on blade pressure sides. Journal of Turbomachinery 111, 284–292.

Metzger, D.E., Dunn, M.G., Hah, C., 1991. Turbine tip and shroud heat transfer. Journal of Turbomachinery 113, 502–507.

Moore, J., Moore, J.G., Henry, G.S., Chaudhry, U., 1989. Flow and heat transfer in turbine tip gaps. Journal of Turbomachinery 111, 301–309.

Nasir, H., Ekkad, S.V., Kontrovitz, D.M., Bunker, R.S., Prakash, C., 2004. Effect of tip gap and squealer geometry on detailed heat transfer measurements over a high pressure turbine rotor blade tip. Journal of Turbomachinery 126, 221–228.

Newton, P.J., Lock, G.D., Krishnababu, S.K., Hodson, H.P., Dawes, W.N., Hannis, J., Whitney, C., 2006. Heat transfer and aerodynamics of turbine blade tips in a linear cascade. Journal of Turbomachinery 128, 300–309.

Papa, M., Goldstein, R.J., Gori, F., 2003. Effects of tip geometry and tip clearance on the mass/heat transfer from a large-scale gas turbine blade. Journal of Turbomachinery 125, 90–96.

Rhee, D-H., Cho, H.H., 2006a. Local heat/mass transfer characteristics on a rotating blade with flat tip in a low-speed annular cascade-Part I: near-tip surface. Journal of Turbomachinery 128, 96–109.

Rhee, D-H., Cho, H.H., 2006b. Local heat/mass transfer characteristics on a rotating blade with flat tip in a low-speed annular cascade-Part II: tip and shroud. Journal of Turbomachinery 128, 110–119.

Rued, K., Metzger, D.E., 1989. The influence of turbine clearance gap leakage on passage velocity and heat transfer near blade tips: Part II-source flow effects on blade suction sides. Journal of Turbomachinery 111, 293–300.

Sjolander, S.A., Amrud, K.K., 1987. Effects of tip clearance on blade loading in a planar cascade of turbine blades. Journal of Turbomachinery 109, 237–245.

STP 470A, 1974. Manual on the Use of Thermocouples in Temperature Measurement. American Society for Testing and Materials.

Tallman, J., Lakshminarayana, B., 2001. Numerical simulation of tip leakage flow in axial flow turbines, with emphasis on flow physics: part I-effect of tip clearance height. Journal of Turbomachinery 123, 314–323.

Yamamoto, A., 1989. Endwall flow/loss mechanisms in a linear turbine cascade with blade tip clearance. Journal of Turbomachinery 111, 264–275.